



UNIVERSITÀ
DEGLI STUDI
FIRENZE

FLORE

Repository istituzionale dell'Università degli Studi di Firenze

Hybrid nano-composites for the consolidation of earthen masonry

Questa è la Versione finale referata (Post print/Accepted manuscript) della seguente pubblicazione:

Original Citation:

Hybrid nano-composites for the consolidation of earthen masonry / Camerini, Rachel; Chelazzi, David; Giorgi, Rodorico; Baglioni, Piero. - In: JOURNAL OF COLLOID AND INTERFACE SCIENCE. - ISSN 0021-9797. - ELETTRONICO. - 539:(2019), pp. 504-515. [10.1016/j.jcis.2018.12.082]

Availability:

The webpage <https://hdl.handle.net/2158/1147007> of the repository was last updated on 2024-04-29T17:18:14Z

Published version:

DOI: 10.1016/j.jcis.2018.12.082

Terms of use:

Open Access

La pubblicazione è resa disponibile sotto le norme e i termini della licenza di deposito, secondo quanto stabilito dalla Policy per l'accesso aperto dell'Università degli Studi di Firenze (<https://www.sba.unifi.it/upload/policy-oa-2016-1.pdf>)

Publisher copyright claim:

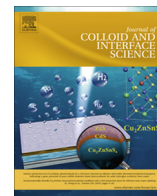
La data sopra indicata si riferisce all'ultimo aggiornamento della scheda del Repository FloRe - The above-mentioned date refers to the last update of the record in the Institutional Repository FloRe

(Article begins on next page)



Contents lists available at ScienceDirect

Journal of Colloid and Interface Science

journal homepage: www.elsevier.com/locate/jcis

Regular Article

Hybrid nano-composites for the consolidation of earthen masonry

Rachel Camerini, David Chelazzi, Rodorico Giorgi*, Piero Baglioni*

CSGI and Department of Chemistry, University of Florence, via della Lastruccia 3-50019, Sesto Fiorentino, Italy



GRAPHICAL ABSTRACT



ARTICLE INFO

Article history:

Received 13 November 2018

Revised 20 December 2018

Accepted 21 December 2018

Available online 22 December 2018

Keywords:

Nano-composites

Calcium silicate hydrate

Silica

Calcium hydroxide

Hydroxypropyl cellulose

Earthen masonry

Adobe

Consolidation

Heritage preservation

ABSTRACT

Hypothesis: Earth is one of the oldest silicate-based materials in stone heritage, still largely used in architecture worldwide. Earthen materials are highly susceptible to wind and water erosion, leading to loss of cohesion and crumbling. Conventional consolidants (alkoxysilanes, synthetic or natural polymers) lack physico-chemical compatibility or effectiveness, and can promote degradation. We propose for the first time nano-composites for the surface consolidation of adobe, i.e. unbaked earth bricks often containing organic fibers and lime.

Experiments: We investigated, mimicking the setting of portland cement, the formation of calcium silicate hydrate (CSH) within adobe porosities, owing to the pozzolanic reaction between nanoparticles of silica and calcium hydroxide, to consolidate a powdery substrate. Different formulations were characterized by Fourier Transform Infrared spectroscopy (FTIR), X-ray diffraction (XRD), scanning and transmission electron microscopy (SEM, TEM), dynamic light scattering (DLS), and turbidimetry (UV–Vis spectroscopy).

Findings: A ternary composite made of SiO_2 nanoparticles, $\text{Ca}(\text{OH})_2$ nanoparticles, and hydroxypropyl cellulose, dispersed in a (4:1) ethanol:water blend, was formulated. Each component is compatible with adobe, and plays a role in its consolidation. The treatment of adobe samples with the composite leads to the *in situ* formation of CSH, providing resistance to peeling, abrasion, and wet-dry cycles, with no aesthetic alteration. This opens new perspectives in the preservation of one of the most widely used construction materials.

© 2018 Elsevier Inc. All rights reserved.

* Corresponding authors.

E-mail addresses: camerini@csgi.unifi.it (R. Camerini), chelazzi@csgi.unifi.it (D. Chelazzi), giorgi@csgi.unifi.it (R. Giorgi), baglioni@csgi.unifi.it (P. Baglioni).

1. Introduction

Siliceous stones represent a wide and important material class in artistic and architectural heritage. These materials share a silicate-based matrix, but have extremely diversified compositions and structures, including both natural lithoids (from granite to sandstone) and artificial materials like ceramic products and cement. Among silicate-based substrates, earthen masonry (i.e. building materials obtained with an unfired mixture of soil and water) has been used since antiquity owing to its cheapness and availability, simple manufacturing process, good thermal and acoustic properties, and ecofriendliness. Nowadays, earthen masonry is diffusing in many industrialized countries (sustainable architecture). Currently, over half of the world's population lives in unbaked earth houses, as estimated by the United States Department of Energy [1]. The earthen architectural heritage includes immovable patrimony ranging from archaeological sites to modern buildings. The typical outdoor location of these artifacts requires continuous conservation interventions specifically addressed to the type of substrate and degradation.

Among earthen materials, adobe is of great archaeological and architectural interest [2,3]. Adobe bricks are handmade, obtained by mixing earth and water, and then sun drying the mixture. Recipes and mineralogical composition of soils are various, according to local traditions and materials availability. In order to avoid cracking during drying and optimize the bricks' strength, the mixture can be adjusted by re-proportioning the soil fractions, or by adding stabilizers, especially natural organic fibers (straw, dry grass) [4–6] or artificial products, often including lime in small percentages [7,8]. Adobe is particularly susceptible to wind and water erosion, and degrades easily. The prolonged circulation of water in the adobe pores induces washouts, freeze-thaw cycles, and swelling-shrinkage cycles of the clay fraction, leading to progressive reduction of the grains' cohesion, loss of mechanical properties, and eventually crumbling (Fig. 1). The availability of effective consolidants able to restore the cohesion of adobe artifacts, would help the preservation of an immense patrimony. However, conventional consolidants and adhesives, commonly used in restoration, exhibit several limitations and drawbacks [9]. Natural organic polymers have limited durability and effectiveness: plant mucilage (primarily cactus) is largely used in Mesoamerican regions, but it ages rapidly, requiring frequent treatments [1]; synthetic polymers are often physico-chemically and esthetically incompatible [10,11], and can undergo degradation and discoloration [12–14]. In most cases, polymers have to be removed with sophisticated methodologies [15–17], in order to protect the works of art from enhanced degradation. Alkoxysilanes solutions, commonly used on silicate stone, are known to form brittle xerogels

susceptible to cracking, due to the high capillary pressures developed in the microporous network during drying [18,19]. Currently, valid alternatives to traditional consolidants for earthen materials, and in particular adobe, are still lacking.

Advancements in colloids and materials science have provided candidate materials to fill this gap. For instance, sols have been obtained using silica oligomers and surfactants, and applied to stone consolidation [20], and aqueous solutions of colloidal silica nanoparticles have been investigated as consolidants, inquiring the effect of relative humidity on the treatment of siliceous-carbonate stone [21]. Nanoparticles of $\text{Ca}(\text{OH})_2$ have been successfully used for the consolidation of wall paintings, plaster and stone (not only carbonate); these nanoparticles can be stably dispersed in short chain alcohols up to high concentrations, and several approaches have been proposed in the last decades concerning their synthesis and application [22–25].

In the present contribution, we aimed to obtain consolidation of adobe by exploiting the *in situ* formation of calcium silicate hydrate (CSH), responsible for the hardening of cement, one of the most largely used construction materials [26]. The interaction of silica with calcium hydroxide, yielding CSH phases, has been widely studied in the past [27–31], and the alkaline activation of bulk silica with aqueous solutions of hydroxides was considered for the restoration of adobe [10]. However the effectiveness of the process was poor due to the micrometer size of the particles, i.e. the low surface area available for the CSH formation that could be enhanced when both silica and calcium hydroxide are in the form of nanoparticles. The possibility of preparing dispersions of nanoparticles in different solvents (besides water, short chain alcohols and water-alcohol blends) opens new perspectives for earthen materials consolidation. These systems are less prone than conventional water-based particles dispersions to sedimentation, aggregation, and detrimental effects caused by excessive wetting of earthen materials with water (freeze-thaw cycles, transport of soluble salts, growth of microorganisms [32]). Recently, Rodríguez-Navarro et al. observed the consolidation of sandstone after the application of nanolime dispersions, hypothesizing that the reaction between the dispersions and silica grains in the stone might lead to the formation of a gel similar to CSH phases [23]. Daniele et al. investigated the interaction of silica fume with $\text{Ca}(\text{OH})_2$ aqueous suspensions stabilized by a non-ionic surfactant (Triton X-100) [33], reporting on the formation of CSH phases. However, the use of purely aqueous systems involves the aforementioned drawbacks in practical applications on stone, besides the use of surfactants as stabilizers is discouraged, as the long-term behavior of these additives on the stone substrate has not yet been investigated.

The aim of the present paper is to develop CSH *in situ* for the consolidation of adobe, starting from silica and $\text{Ca}(\text{OH})_2$, two major



Fig. 1. An adobe brick from the Morelos state (Mexico) showing poor mechanical properties: crumbling and loss of grains occur just by touching.

components of the cement chemistry. The two components are in the form of nanoparticles to burst their reactivity. The formation of CSH is further enhanced by the addition of *Klucel*, hydroxypropyl cellulose, in the formulation. In fact, cellulose ethers (CEs) constitute an important class of organic polymers used in cement formulations. They are used in the cement industry as anti-washout or water-proofing admixtures, for the production of adhesive mortars, as viscosity-modifiers, and to control the workability of cement (i.e. the drying time). In this paper *Klucel* performs three main actions: (i) acts as a viscosity-modifier; (ii) cellulose based materials are typically used in adobe preparation to provide flexural strength and reduce hygrometric shrinkage during drying, and are commonly used in restoration practices as adhesives, densifiers, and additives for earthen grouts [4,34,35]; (iii) cellulose additives act as regulators of water release during the whole hydration reaction, increasing the hydration efficiency, and promoting the formation of CSH [26,36]. The three components were dispersed in a (4:1) ethanol:water blend. Ethanol was selected as it is an optimal solvent in terms of volatility, surface tension, and boiling point, for the application of nanoparticles to mortars and stone [37]. The amount of water was reduced, maintaining a water content suitable for the setting of CSH phases.

The composite system was characterized through Fourier Transform Infrared spectroscopy (FTIR), X-ray diffraction (XRD), scanning and transmission electron microscopy (SEM, TEM), dynamic light scattering (DLS), and turbidimetry (UV–Vis spectroscopy). The composite was then applied to adobe mock-ups, assessing the penetration depth of the formulation, the change in the color, mechanical properties and water sorption of the treated samples.

2. Materials and methods

2.1. Materials

Nanosilica dispersions were prepared diluting in water (down to 10 g/L) the commercial product Levasil CS40-213 (Akzo Nobel Chemicals), i.e. monodisperse spheres of amorphous SiO_2 (original concentration of 40 wt% in water, 0.2 wt% of Na_2O as stabilizer), particle size of 25 nm, specific surface area of 130 m^2/g , pH 9, hereinafter reported as SiO_2 . The pH of the diluted nanosilica dispersion is 7. An ethanol dispersion of $\text{Ca}(\text{OH})_2$ nanoparticles (hereinafter *lime*) was produced via solvothermal reaction as reported in the literature [38]. The synthesis yields hexagonal platelets of portlandite of ca. 200 nm, at a concentration of 35 g/L, which was diluted to 5 g/L. An ethanol solution of a commercial hydroxypropyl cellulose (hereinafter *HPC*) (*Klucel*[®]-G, 300 mPas, Phase Restauro) was prepared at a concentration of 20 g/L. Ethanol (ACS grade) was purchased by Fluka. Water was purified by a Millipore Milli-Q UV system (resistivity >18 $\text{M}\Omega\text{ cm}$).

2.2. Preparation of the ternary formulation

The ethanol dispersion of $\text{Ca}(\text{OH})_2$ nanoparticles was added to a mixed ethanol solution of hydroxypropyl cellulose-silica aqueous dispersion. The mixed system (SiO_2 -*HPC*-*lime*) was kept under stirring for 6 h. Different formulations were tested; the one selected for application and assessment on adobe mock ups is a hydroalcoholic dispersion (ethanol:water = 4:1% v/v) with concentrations of 2.5, 2.5 and 5 g/L for SiO_2 , *lime* and *HPC* respectively (SiO_2 : *lime* : *HPC* = 1:1:2% w/w). These concentration values were selected to maximize the consolidation effect while maintaining the stability of the composite system (i.e. avoid sedimentation). The liquid medium of the ternary formulation is alkaline (the pH-meter gave values higher than 12).

2.3. Characterization of the components and the formulation

The possible formation of new phases in the ternary composite was investigated via morphological and compositional analyses, namely Attenuated Total Reflectance Fourier Transform Infrared Spectroscopy (ATR-FTIR), X-ray diffraction (XRD) and Scanning Electron Microscopy (SEM). ATR-FTIR was performed using a Thermo Nicolet Nexus 870 spectrometer equipped with a liquid nitrogen-cooled Mercury Cadmium Telluride detector, a single reflection diamond crystal ATR unit, and a Golden Gate diamond cell. The spectra were acquired in the 4000–650 cm^{-1} range with a spectral resolution of 4 cm^{-1} .

XRD was carried out using a D8 Bruker “Da Vinci” diffractometer equipped with a primary Ge monochromator using for Cu $\text{K}\alpha 1$ radiation ($\lambda = 1.54 \text{ \AA}$) and a Sol-X solid state detector in Debye-Scherrer geometry (2θ range of 5–60°, step size of 0.02°, time/step of 0.3 s, voltage of 40 kV and current of 40 mA). For FTIR and XRD, the samples were air-dried and grinded prior to measurement.

For SEM investigations, the dispersions were deposited on the stub and let dry prior to measurement with a field emission gun scanning electron microscope (FEG-SEM), SIGMA (Carl Zeiss, Germany) with acceleration potential of 25 kV and a working distance of 8.6 mm.

In order to further investigate the mutual interaction of the components, the single dispersions/solutions (SiO_2 , *lime*), their binary combinations (SiO_2 -*lime*, SiO_2 -*HPC* and *HPC*-*lime*) and the ternary system (SiO_2 -*HPC*-*lime*) were characterized by dynamic light scattering (DLS). Measurements on the single components were also carried out at the same concentrations of the ternary composite system (e.g. SiO_2 was diluted down to a concentration of 2.5 g/L in a 4:1 ethanol/water ratio); these samples are indicated as SiO_2T , and *limeT*. The particle size distribution and ζ -potential were determined using a 90Plus Particle Size Analyzer (Brookhaven Instruments), with incident 659 nm laser light radiation, and collection at 90°. The measurements were recorded at 25 °C. For the particle size measurements, the systems were diluted 1:10. The values reported are the average of three measurements consisting of 5 runs of 30 s. The refractive index of the liquid medium (ethanol:water blend 4:1) is 1.36 [39,40]; the presence of the highly diluted cellulose derivative dissolved in the blend (*Klucel*[®]-G, 0.5 g/L) was not considered as relevant for the measurements. For the solid content of the dispersions, the average of the indexes of the components (SiO_2 , $\text{Ca}(\text{OH})_2$) was used. The CONTIN method was used for fitting the autocorrelation functions, to obtain the particle size distributions. The data are intensity-weighted. For the ζ -potential measurements, the Smoluchowski equation was used for the fitting of the autocorrelation function. The systems were also observed using Transmission Electron Microscopy (TEM), with a STEM CM12 Philips electron microscope. The samples were cast onto a carbon-coated copper grid sample holder, followed by evaporation of the solvent at room temperature.

The pH of the SiO_2 aqueous dispersion was measured using a glass electrode pH-meter (Crison-Basic20): the reported value is the average of three measurements.

The kinetic stability of the dispersions (SiO_2 , *lime*, all the binary systems and the ternary system) was investigated via turbidimetric analysis, performed with a Cary Bio 100 UV–VIS spectrophotometer (Varian). The absorbance at $\lambda = 600 \text{ nm}$ (spectral band width = 1 nm) was recorded at 25 °C as a function of time, at regular time intervals, over a total period of 1 month, using sealed quartz cuvettes with an optical path of 1 cm. Decreases in the absorbance were ascribed to the formation of aggregates and sedimentation. The values reported are the average of five measurements.

2.4. Treatment of the adobe samples

As target material of our study, we used adobe bricks from the Morelos state (Mexico), originally prepared using local soil and straw fibers. The bricks ($5 \times 10 \times 20 \text{ cm}^3$) were cut with an abrasive disc saw into smaller specimens with dimensions of $4 \times 4 \times 2 \text{ cm}^3$ and average weight of 40 g.

The treatment of adobe was performed by soaking each specimen with 20 mL of ternary formulation ($\text{SiO}_2\text{-HPC-lime}$). The specimens were placed in a container previously filled with the formulation, and kept there until complete absorption (ca. 1 day). Then, the specimens were stored under room conditions ($T = 23^\circ\text{C}$, $\text{RH} = 50\%$) until characterization. For comparison, the same treatment was performed using the single components and the binary combinations $\text{SiO}_2\text{-HPC}$ and HPC-lime . The treatment with the binary $\text{SiO}_2\text{-lime}$ was not performed due to immediate particle flocculation, see below.

2.5. Characterization of the adobe samples

Before treatment, the grain size distribution of the adobe soil was characterized according to the Standard Test Method for particle-size analysis of soils (ASTM D422-63) and the Standard Test Method for particle-size distribution of fine-grained soils, using sedimentation analysis (ASTM D7928-16). The Atterberg Limits were also obtained (Liquid Limit – BS 1377:1975 and Plastic Limit – ASTM D 4318-93), and the Plastic Index was then calculated. The carbonates content was determined using a Dietrich-Fruhling calcimeter, and the organic content was determined by the C–N–H determination method. XRD was also carried out to investigate the mineralogical composition of the soil.

Two months after the treatment, the treated (T) and non-treated (NT) adobe specimens were characterized to assess the consolidation efficacy. Colorimetric analyses were performed using an X-Rite SP60 portable colorimeter, (D65/10°, 8 mm diameter circular measuring spot), to evaluate the possible color changes produced by the application of the formulation. The experiment was performed on four areas of three different samples. The color difference between the treated and non-treated samples was calculated using the formula $\Delta E^* = \sqrt{\Delta L^{*2} + \Delta a^{*2} + \Delta b^{*2}}$, where L^* , a^* and b^* are the coordinates of the CIE 1976 color space. ATR-FTIR, XRD, and the phenolphthalein test [24] were used to assess the penetration and distribution of the applied product, and to verify the occurrence of consolidation reactions within the substrate. Scotch tape tests, abrasion tests, wet-dry cycles, water sorption measurements, and drilling tests were carried out on the adobe samples.

The scotch tape test (or peeling test) is a common method used in conservation practice for the evaluation of the efficacy of consolidation treatments in terms of restoration of the surface cohesion properties [41]. The test consists in pressing pieces of adhesive tapes of known weight and area on the sample surface, and peel them off after few minutes. The decohesion index, DI (mg/cm^2), is the weight of the material lost per unit area, and is inversely proportional to the grains' cohesion forces. The data reported are the average of measurements performed on four areas of the sample, for three different samples. The experiment was conducted three times on each area, in order to obtain the decohesion index following the progressive removal of surface layers. The total removed mass over the three experiments was also calculated.

The abrasion test [42,43] consists in subjecting the sample to mechanical erosion by brushing with a metal brush at a constant pressure (3 kg mass on the top center of the brush), for a given number of cycles (in this case three cycles, each consisting of 60 rounds of brushing in one minute), over the entire length of the

specimen. The abrasion coefficient, A_c (cm^2/mg), expresses the ratio of the surface to the quantity of the material removed by brushing, and is proportional to the abrasive strength. The data reported are the average of tests performed on three samples; the total value after the three cycles was also calculated.

Wet-dry cycles were performed to assess the resistance to exposure to harsh environmental cycles [43,44], by immersing the samples in distilled water for 5 h and drying at 60°C for 48 h. Seven cycles were performed, and the weight loss was expressed as the percentage of dry mass reduction from the original mass, as the average of the data obtained from two samples. The total value after the seven cycles was also calculated.

For the water sorption measurements, the samples were oven-dried at 60°C to constant mass, weighted and put on a porous support in contact with distilled water. The water intake is measured indirectly by weighting the samples at regular time intervals. The capillary water absorption coefficient, A_w ($\text{mg}/\text{cm}^2 \cdot \text{s}^{1/2}$), of the treated and untreated samples was obtained using the 'one tangent method', i.e. calculating the gradient of the straight line obtained by plotting the cumulative mass of water absorbed per unit area against the square root of time [45,46]. The experiment was repeated twice.

The drilling tests [47] were carried out with a drilling resistance measurement system (Sint Technology, Italy), using a 5 mm diameter drill bit (maximum depth = 10 mm, penetration rate = 20 mm/min, revolution speed = 200 rpm). Each result is the average of three holes produced on two different samples.

3. Results and discussion

3.1. Characterization of the components and formulation

In order to gain information on the interaction between $\text{Ca}(\text{OH})_2$ and silica nanoparticles, namely on the formation of CSH phases, ATR-FTIR and XRD analyses were performed on the ternary system $\text{SiO}_2\text{-HPC-lime}$.

ATR-FTIR analyses were performed on the formulation as prepared, and after 6 days, 9 days, and 2 months from preparation (Fig. 2), according to the procedure above reported. All the FTIR spectra of $\text{SiO}_2\text{-HPC-lime}$ show a broad band centered at 3400 cm^{-1} and a small band at 1650 cm^{-1} assigned to the stretching and bending of the hydroxyl groups of HPC, residual $-\text{OH}$ groups in silica, and adsorbed water. The characteristic peak around 3640 cm^{-1} (OH stretching) indicates the presence of calcium hydroxide. The latter is partially converted into calcium carbonate through reaction (carbonation) with atmospheric CO_2 , during air-drying of the sample [23,38,48], as indicated by the presence of bands at $1400\text{--}1500$ (ν_3 asymmetric CO_3 stretching), 876 (ν_2 asymmetric CO_3 bending), and 713 cm^{-1} (ν_4 symmetric CO_3 bending) [49,50], which are present in the spectra collected on the formulation as prepared, and after 6 and 9 days from preparation. Calcium hydroxide and calcium carbonate bands are absent in the spectrum collected after two months from preparation. The bands between 2970 and 2870 cm^{-1} (C–H stretching) in the four spectra can be ascribed to HPC. Bands between 1460 and 1270 cm^{-1} (C=C stretching) are also ascribable to HPC; while the band of HPC at 1075 cm^{-1} (C–O stretching) [51,52] overlaps with the absorption at 1050 cm^{-1} of silica (internal Si–O–Si asymmetric stretching) that also displays a band at 800 cm^{-1} (Si–O–Si symmetric stretching). The shoulder at 950 cm^{-1} is assigned to the Si–O stretching of surface Si–OH groups [53,54]. Interestingly, the spectra of $\text{SiO}_2\text{-HPC-lime}$ collected after 9 days and, more evidently, after two months from preparation, show a marked increase of the band at 950 cm^{-1} and a correspondent decrease of the band at 1050 cm^{-1} , indicating the breakage of Si–O–Si

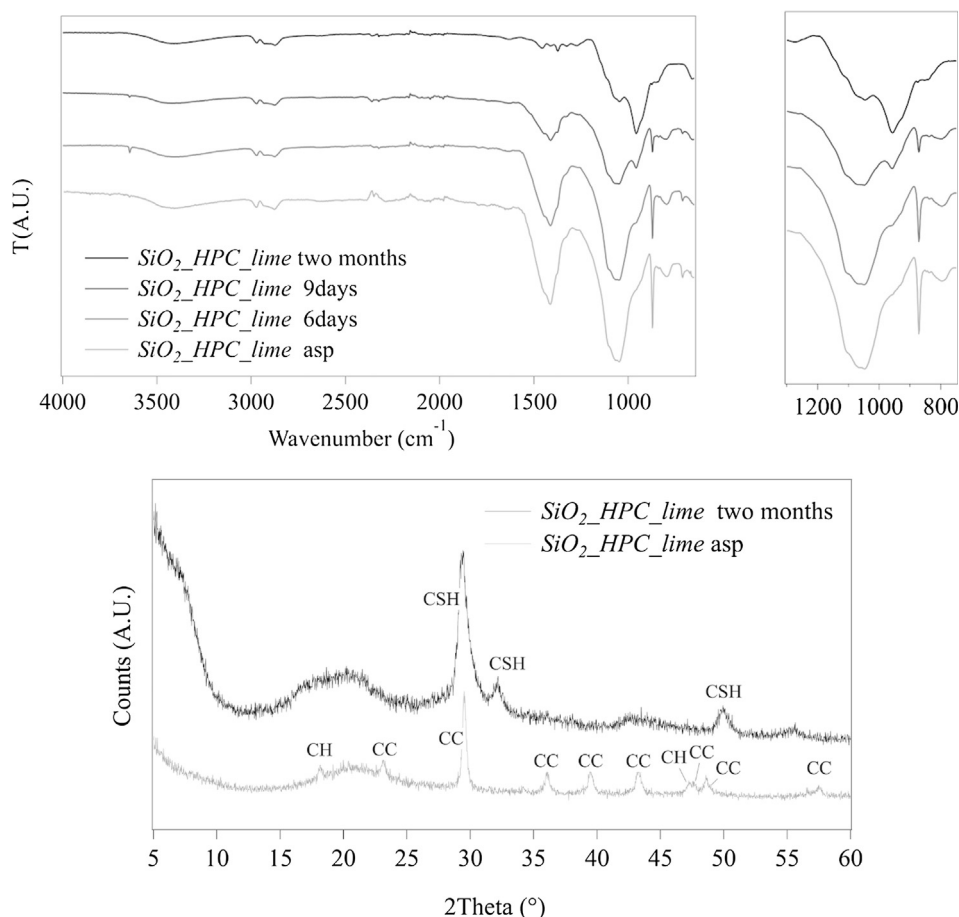


Fig. 2. (Top) ATR-FTIR spectra of air-dried ternary system $\text{SiO}_2\text{-HPC-lime}$ as prepared (“asp”), and 6 days, 9 days and two months after preparation; (bottom) XRD patterns of air-dried ternary system $\text{SiO}_2\text{-HPC-lime}$ as prepared and two months after preparation.

bonds and the formation of silanol groups. This suggests that silica depolymerization and the formation of calcium silicate hydrate (CSH) occurred [30,31,55]. In fact, it is reported that the hydration reaction between $\text{Ca}(\text{OH})_2$ and silica in water starts with the dissolution of $\text{Ca}(\text{OH})_2$ followed by the breaking of the Si—O—Si covalent bonds by the released OH groups; the Ca^{2+} ions then bridge the depolymerized silica, forming the basic units of CSH [56]. After two months, the absence of calcium hydroxide and carbonate bands in the spectrum indicates the complete reaction of calcium hydroxide and silica nanoparticles. Besides, after two months, the formation of a gel-like phase is macroscopically observed in the ternary formulation. A similar behavior was observed in the $\text{SiO}_2\text{-lime}$ system, but not in the other binary systems or for single components in the hydro-alcoholic blend; thus, we concluded that the gel consisted of the newly formed CSH phase.

XRD analysis was carried on the ternary system as prepared, and two months after preparation. In the first case, the peaks of calcium hydroxide and calcium carbonate are observed, along with a broad band centered around 20° , ascribable to the co-presence of amorphous silica (reported at 22° in the literature [53]) and HPC (band at 17° [52]). After two months, three peaks are observed at 29.5° , 32° and 50° , indicating the formation of CSH [30,57,58]. Basal peaks at less than 10° are reported in the literature for tobermorite, but their intensity can vary depending on the type of CSH phase, up to being barely or not observable [59,60].

The SEM investigation of the ternary system after two months from preparation, showed the presence of a homogeneous porous network of crumpled foils (Fig. 3), a morphology typically produced by the formation of CSH from the alkaline activation of

nanosilica [31,61]. The EDX analysis confirmed that calcium and silicon are homogeneously distributed across the foiled substrate.

To further investigate the components' behavior and their mutual interactions, the ζ -potential and particle size of the single components (SiO_2 , lime, HPC), their binary systems, and the ternary system were then analyzed, and the results are reported in Table 1. The reported values are those of the as prepared samples. The CONTIN method was used to fit the autocorrelation functions, and the data are intensity-weighted. The mean particle size and relative variance (i.e. ratio of variance to the square of the mean, which is a measure of the polydispersity of diffusion coefficient, and is often represented as a polydispersity index) are reported. The main populations of multimodal distributions are also indicated. Transmission Electron Microscopy (TEM) was also used to observe the air-dried samples.

In the case of SiO_2 and lime, the data are in agreement with the literature [38,62,63] and the information provided by producers: the silica nanoparticles (monodisperse spheres) exhibit in water a negative ζ -potential close to -30 mV, indicating a stable colloidal system due to electrostatic repulsion, and an average hydrodynamic diameter of 33 nm with a relative variance of 0.03, which is in agreement with the particles' size observed with TEM (25–35 nm, see Fig. 4). The pH of SiO_2 system is 7, i.e. after dilution of the original product Levasil CS40-213.

The synthesized $\text{Ca}(\text{OH})_2$ nanoparticles (hexagonal platelets) in ethanol have a positive ζ -potential of about 50 mV, consistent with the good stability of the system, and a mean particle size of 214 nm (relative variance of 0.16). This is in agreement with the presence of two main populations centered at about 15 and 175 nm as also

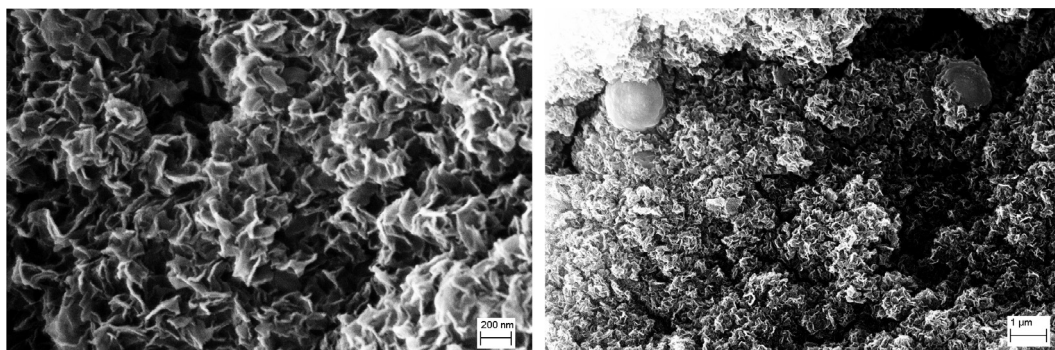


Fig. 3. SEM images of the ternary system $\text{SiO}_2\text{-HPC_lime}$, air-dried after two months from preparation (secondary electron images with magnitude of (a) 21kX and (b) 87kX).

Table 1

ζ -potential and particle size data of the different components and composite formulations, obtained by dynamic light scattering measurements.

System	Medium	ζ -potential (mV \pm SD)	Particle size		
			Mean particles' size (nm)	Rel. Var.	Distribution
SiO_2	H_2O	-29 ± 7	33	0.03	Monomodal, narrow
lime	EtOH	53 ± 7	214	0.16	Multimodal, main populations at ca. 15 and 175 nm
SiO_{2T}	$\text{H}_2\text{O}/\text{EtOH}$ (1:4)	-43 ± 12	38	0.19	Monomodal, narrow
lime _T	$\text{H}_2\text{O}/\text{EtOH}$ (1:4)	41 ± 3	520	0.81	Monomodal, broad
$\text{SiO}_2\text{-lime}$	$\text{H}_2\text{O}/\text{EtOH}$ (1:4)	n/a	n/a	n/a	Formation of micron-sized aggregates
$\text{SiO}_2\text{-HPC}$	$\text{H}_2\text{O}/\text{EtOH}$ (1:4)	-1 ± 11	95	0.46	Multimodal, main populations at ca. 35 and 160 nm
HPC_lime	$\text{H}_2\text{O}/\text{EtOH}$ (1:4)	-1 ± 8	945	0.25	Multimodal, main populations at ca. 130 and 960
$\text{SiO}_2\text{-HPC_lime}$	$\text{H}_2\text{O}/\text{EtOH}$ (1:4)	-3 ± 9	941	0.16	Multimodal, main populations at ca. 300 and 1050

confirmed by TEM images (see Fig. 4b), with an average thickness of the platelets of 20–30 nm [63].

When the components are dispersed in the (4:1) ethanol-water solution, the ζ -potential and size of the particles change with respect to the systems in the pure media. In particular, the ζ -potential of silica nanoparticles in the blend (SiO_{2T}) has a slightly higher negative value, as expected from the fact that the dielectric constant of the dispersing medium (i.e. the blend) is lower than that of water [64,65]. The particles' size is comparable with that of SiO_2 , but the higher variance (0.19) indicates the presence of some aggregates.

In the case of $\text{Ca}(\text{OH})_2$ nanoparticles, passing from an ethanol dispersion to the blend (lime_T), the dielectric constant increases, and a lower positive ζ -potential is found. It is worth mentioning that the particles' size increases due to the water molecules bridging of the hydroxide platelets, leading to the formation of aggregates [37,66].

The system $\text{SiO}_2\text{-lime}$ could not be analyzed by DLS, as the interaction of the silica and $\text{Ca}(\text{OH})_2$ nanoparticles, whose surface charge is of opposite sign, leads to flocculation and sedimentation of the particles, which occur completely within 24 h from the preparation of the binary system. TEM observation of the system (Fig. 4c) shows the presence of spherical particles with size ranging from 20 to 100 nm corresponding to the SiO_2 component; some of the particles are surrounded by sub-spherical formations whose size ranges from 200 nm up to 1 μm . Such agglomerates (highlighted by arrows in Fig. 4c) might indeed result from the initial interaction of silica and lime nanoparticles.

The binary systems $\text{SiO}_2\text{-HPC}$ and HPC_lime have low ζ -potentials, conceivably related to the presence of hydroxypropyl cellulose. In the literature it is reported that surface adsorption of cellulose ethers (HPC; HEC) onto charged particles resulted in the decrease of ζ -potential, close to zero [67,68], and reduced the agglomeration of the particles due to the formation of a steric barrier. $\text{SiO}_2\text{-HPC}$ shows two different size populations (ca. 35 and 160 nm), with mean particles' size of ca. 95 nm and relative vari-

ance of 0.46, which can be explained by the presence of HPC adsorbed on the surface of the silica particles [69]. TEM observation of the system (Fig. 4d) shows the presence of nanospheres of about 30 nm, which stack into chains or groups of 200–400 nm, in fair agreement with DLS data. In the case of HPC_lime, two population sizes are observed with mean dimension of 945 nm and relative variance of 0.25.

The ternary system $\text{SiO}_2\text{-HPC_lime}$ exhibits a ζ -potential close to zero, as expected for the aforementioned considerations. The system shows two main populations with size of ca. 300 and 1050 nm, with a mean size of 941 nm and a variance of 0.16. This can be explained taking into account the formation of agglomerates of silica and $\text{Ca}(\text{OH})_2$ nanoparticles, and the adsorption of HPC on the agglomerates. TEM analysis (Fig. 4f, g) showed nearly spherical or elongated agglomerates of about 1 μm , formed by the interaction of nanoparticles (less than 100 nm) and fibrous structures.

It is important to notice that the size of the agglomerates is compatible with the average pore size of adobe. In fact, adobe bricks have pore size from micrometric scale up to a few mm, with porosity values of 20–40% [70,71].

Turbidimetric analyses were also performed to gain information on the kinetic stability of the dispersions (i.e. SiO_2 , lime, $\text{SiO}_2\text{-lime}$, $\text{SiO}_2\text{-HPC}$, HPC_lime and $\text{SiO}_2\text{-HPC_lime}$), and the results are shown in Fig. 5. The small size of the silica nanoparticles makes both SiO_2 and $\text{SiO}_2\text{-HPC}$ appear transparent, hence no useful information could be obtained from turbidimetry on those systems. However, in both cases no agglomeration or sedimentation of the particles was observed macroscopically over months (Fig. 5).

Lime has a good turbidimetric stability over 4 weeks, and visual inspection showed that the particles dispersion does not settle even after months, confirming that nanoparticles of $\text{Ca}(\text{OH})_2$ are stable in short chain alcohols, as already reported in the literature [38]. The presence of hydroxypropyl cellulose in the dispersion increases its stability (HPC_lime > lime). This can be explained considering that HPC increases the viscosity of the continuous phase, promoting the stability of the dispersed particles, despite the pres-

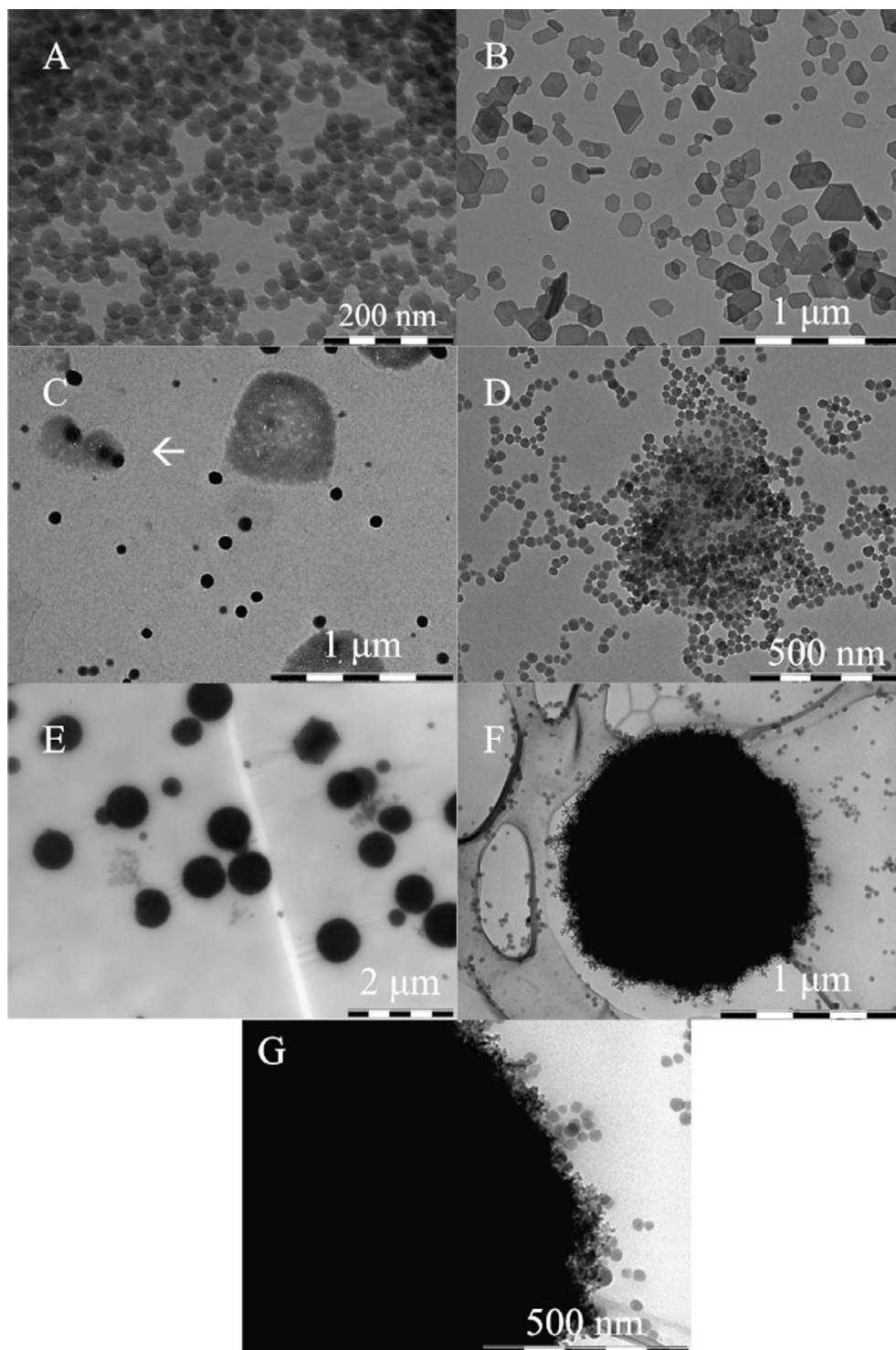


Fig. 4. TEM images of: (a) the silica nanoparticles (SiO_2), (b) the $\text{Ca}(\text{OH})_2$ nanoparticles (*lime*), (c) the binary system SiO_2 _lime, (d) the binary system SiO_2 _HPC, (e) the binary system HPC_lime, and (f, g) the ternary system (SiO_2 _HPC_lime).

ence of larger agglomerates (highlighted by DLS). As expected for the poorly stable SiO_2 _lime system, the absorbance drops from ca. 2 to 0.2 in less than one day.

The absorbance of the ternary system (SiO_2 _HPC_lime) does not change over 4 weeks, as expected for systems containing HPC, confirming the stabilizing role of Klucel®-G in the formulation, which

mediates the interaction between the silica and the lime. After two months, the formation of gel-like phase (ascribed to CSH) occurred as described in the previous paragraphs.

Overall, it was possible to conclude that the formation of CSH takes place in the ternary system (starting about 1 week from the preparation).

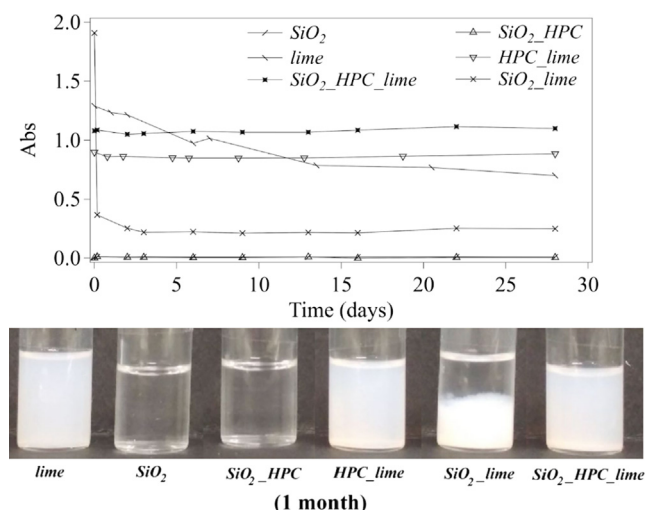


Fig. 5. (Top) turbidimetric analyses performed on *lime*, SiO_2 , $\text{SiO}_2\text{-HPC}$, HPC-lime , $\text{SiO}_2\text{-lime}$, and $\text{SiO}_2\text{-HPC-lime}$, over one month; (Bottom) visual inspections of the $\text{SiO}_2\text{-HPC-lime}$ system as prepared, and after one month from preparation.

3.2. Treatment of adobe samples

Before treatment, the soil of the adobe bricks was characterized, and the results are shown in Table 2. The soil was classified as silty sand (SM), according to the Unified Soil Classification System (USCS). The low clay percentage explains the poor mechanical properties of the samples, as expected considering that the bricks were prepared using local soil from the construction area (Morelos region, Mexico), which has a high content of sand. The XRD analysis of the soil (not shown) revealed a composition consisting predominantly of plagioclases (albite-anorthite) and, to a lesser extent, quartz and mica. Straw fibers were found included in the bricks. The organic content of the soil was found to be ca. 0.3%, and the carbonates content ca. 0.5%.

Visual observations of the samples, up to two months after the treatment, did not highlight significant color variations produced by the application of the formulation $\text{SiO}_2\text{-HPC-lime}$, as compared to the non-treated samples. Colorimetry measurements were then performed, and the analyses showed an average color difference ΔE^* of 2.5 ± 0.5 , which is within the threshold generally adopted for the treatment of works of art, i.e. $\Delta E^* = 3$ [72].

The phenolphthalein test was used to assess the penetration of the calcium hydroxide nanoparticles found in the ternary system, as an indication of the depth reached by the whole formulation. The penetration depth is visually measured thanks to the intense purple color assumed by phenolphthalein at alkaline pH. A 0.1% solution of phenolphthalein was sprayed onto the surface of samples right after treatment. Cross sections of the samples were then cut, and a penetration of 3 mm was observed, which is consistent with that of nanolimes used elsewhere for the consolidation of stucco and adobe [24]. The penetration depth can be affected by several factors including the type of dispersing solvent and the environmental conditions during the treatment, and both backmigration and aggregation of the particles have been discussed as possible issues limiting the penetration [73–78]. While enhancing

the penetration of consolidant particles remains an open topic in stone conservation, it must be noticed that adobe bricks are mainly affected by environmental erosion of the exposed surface, leading to powdering and loss of grains cohesion; thus, the protection of the outer layers up to some mm from the surface was deemed as an acceptable result at this preliminary stage.

FTIR analyses (not shown) were carried out on the treated samples at different depths from the surface, two months after treatment. The characteristic band of calcium hydroxide at ca. 3640 cm^{-1} was not observed, suggesting that the hydroxide had completely reacted, possibly through formation of CSH and carbonation. Bands of calcium carbonate were indeed observed at $1400\text{--}1500$, 876 , and 713 cm^{-1} . However, owing to the intense bands of the silica originally found in the adobe samples, it was not possible to observe an intensity inversion between the band at 950 cm^{-1} (Si–O stretching of surface Si–OH groups) and that at 1050 cm^{-1} (stretching of Si–O–Si bonds), previously ascribed to the depolymerization of the nanosilica particles in $\text{SiO}_2\text{-HPC-lime}$ and the formation of CSH.

Instead, the XRD pattern of powders collected from the treated adobe samples up to 3 mm from the surface, showed peaks at 31.5° , 33.7° and 50.1° (Fig. 6). Interestingly, these peaks exhibit a slight shift to higher angles, and are more resolved, as compared to those observed when CSH is formed in the ternary formulation (see Fig. 2), which might suggest the formation of different calcium silicate hydrate phases, when the process takes place within the pores of the adobe samples. According to the literature, the calcium silicate hydrate minerals tobermorite ($\text{Ca}_5\text{Si}_6\text{O}_{16}(\text{OH})_2 \cdot 4\text{H}_2\text{O}$) and jennite ($\text{Ca}_3\text{Si}_6\text{O}_{18}(\text{OH})_6 \cdot 8\text{H}_2\text{O}$) show diffraction patterns with maxima in the $28.8\text{--}33.2^\circ$ region and at 50.7° , with sharper or broader peaks depending on the degree of order of the phases and the size of the crystallites in the layer plane [58]. It must be noticed that when the formulation sets in the pores of adobe, the original silica component of adobe is present along with the SiO_2 nanoparticles, and a lower Ca/Si ratio is present than when CSH formation takes place entirely in the formulation environment, which might play a role in the formation of CSH phases with different characteristics.

The reaction between SiO_2 and $\text{Ca}(\text{OH})_2$ nanoparticles is known to depend on several factors, including the phase composition and size of the silica nanoparticles, the $\text{Ca}(\text{OH})_2$ content, and the liquid to powder (L/P) ratio of the system [56]. A key factor is the reactivity of the nanosilica with $\text{Ca}(\text{OH})_2$, which is expected to be enhanced when the hydroxide particles have high surface area. In the presence of water, the SiO_2 nanoparticles come in contact with a saturated $\text{Ca}(\text{OH})_2$ solution, which acts as an activator for the breakage of the Si–O–Si bonds, followed by the formation of the cementing phase. It has been shown that when the L/P is 1 mL/g, and for a Ca/Si ratio of 3 (using nanosilica and micron-sized lime particles), the setting of CSH takes place between 1 and 2 h from activation [56]. In our case, the ternary system was applied on the adobe samples 6 days after its preparation: the samples were soaked in the system for 1 day, and then left curing at room conditions ($T = 23^\circ\text{C}$, $\text{RH} = 50\%$). Drying of the samples took 2 more days. The permanence time of the formulation within the pores of adobe seemed to be enough to allow the formation of some CSH phases. HPC is expected to regulate water release, promoting CSH formation; in fact, water proton nuclear magnetic

Table 2

Granulometric characterization of the soil, Atterberg limits (Liquid Limit, LL; Plastic Limit, PL; Plasticity Index, PI), organic content and carbonate content.

Granulometry				Atterberg limits			Organic content (%)	Carbonates content (%)
Clay (%) d < 0.002 mm	Silt (%) d 0.002–0.06 mm	Sand (%) d 0.06–2 mm	Gravel (%) d > 2 mm	LL (%)	PL (%)	PI (%)		
0.1	23.5	74	2.5	33	26	7	0.3	0.5

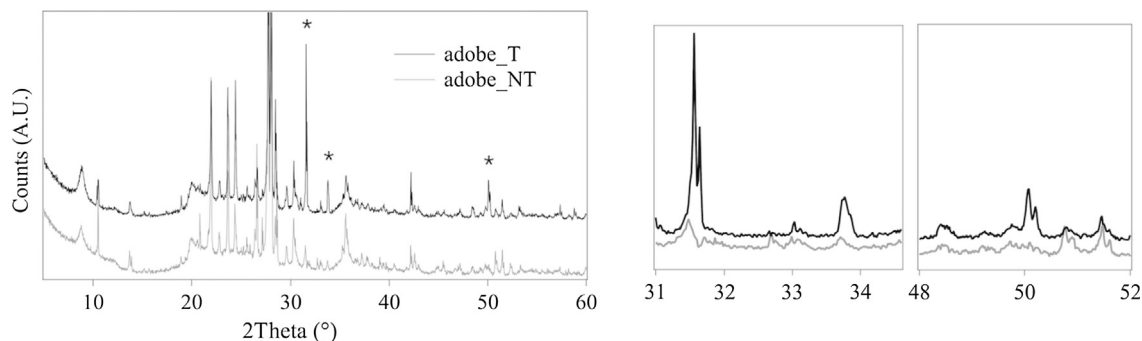


Fig. 6. XRD pattern of untreated (NT, grey line) and treated adobe (T, black line); the insets (31–34° and 48–52°) highlight the peaks at 31.5°, 33.7° and 50.1° found in the patterns of the treated adobe samples, which were assigned to CSH phases.

resonance relaxation experiments showed that cellulosic additives interact with water, determining its availability in the cement hydration process. It was found that cellulosic polymers delay the setting process while, on the other hand, they enhance the hydration efficiency. This was explained considering the hydrophilic character of the cellulose derivative, which is able to bind water, adsorb on silicate grains, and then distribute water homogeneously over the solid phase [26,36,79]. The presence of the cellulosic polymers affects both the nucleation and growth rates of the hydrated phases; namely, the nucleation rate is reduced (even though the energy threshold to form CSH nuclei remains unaltered), while the growth rate increases in the presence of the polymers (the energy threshold to start the growth of the nuclei is lowered) [36].

Applicative protocols should be developed for the treatment of adobe bricks in real case studies, carried out through spraying or brushing. Such protocols should guarantee that the amount of water necessary to trigger the formation of CSH is maintained within the stone pores after the treatment even in dry and hot environments. For instance, humid (not dripping) poultices (e.g. cellulose pulp) could be applied to the surface in order to keep humidity high enough, without loading large amounts of water in the pores [37].

The scotch tape test showed a remarkable increase of cohesion for the adobe samples treated with $\text{SiO}_2\text{-HPC_lime}$. The positive effect was observed even when the peeling was repeated on the same portion of the sample's surface, up to three times. The average values of each of the three peeling cycles are shown in Fig. 7; the total values after the three cycles are reported in Table 3.

Further proof of the consolidation effect was obtained with abrasion tests and wet/dry cycles, performed to assess the response of the treated samples to harsh environmental conditions (wind and water erosion). The values reported in Table 3 and Fig. 8 show a higher abrasion coefficient for the samples treated with $\text{SiO}_2\text{-HPC_lime}$, indicating improved resistance to abrasion. The average values of each cycle, obtained from tests on three different samples, are shown in the graph; the total values after the three cycles are reported in the table.

The average weight losses of untreated and treated samples caused by wet/dry cycles are shown in Fig. 9, and the total weight loss after the seven cycles is reported in Table 3. The results indicate that the application of the $\text{SiO}_2\text{-HPC_lime}$ system resulted in a decrease of mass loss upon repeated immersions in water, indicating that consolidation took place. The capillary sorption coefficient obtained from water sorption measurements did not significantly change following the treatment of the samples

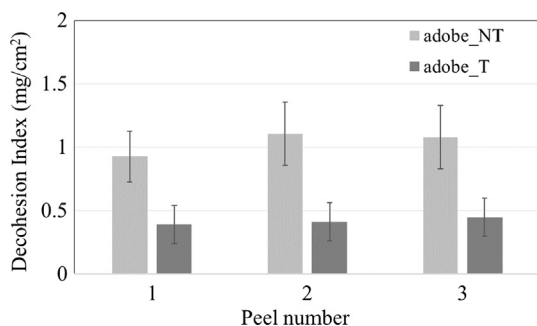


Fig. 7. Decohesion index (obtained with the scotch tape test) of adobe samples, untreated (NT), and treated with $\text{SiO}_2\text{-HPC_lime}$ (T).

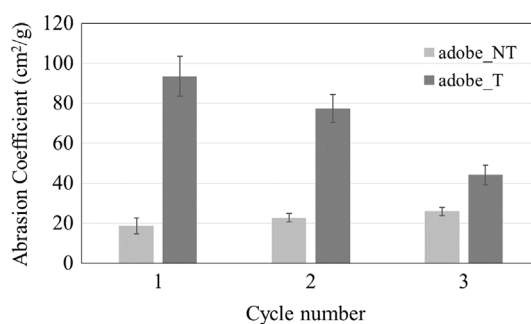


Fig. 8. Abrasion coefficient of adobe samples, untreated (NT), and treated with $\text{SiO}_2\text{-HPC_lime}$ (T).

Table 3

Characterization of adobe samples, untreated (NT), and treated with $\text{SiO}_2\text{-HPC_lime}$ (T).

	Total decohesion index after 3 peels (mg/cm ²)	Total abrasion coefficient after 3 cycles (cm ² /g)	Total weight loss after 7 wet/dry cycles (%)	Capillary sorption coefficient (mg/cm ² ·s ^{1/2})	Drilling resistance (N)
Adobe_NT	3.1 ± 0.6	67 ± 3	4.41 ± 0.12	18.4 ± 0.2	0.88 ± 0.31
Adobe_T($\text{SiO}_2\text{-HPC_lime}$)	1.2 ± 0.2	215 ± 7	0.74 ± 0.04	18.9 ± 0.4	1.07 ± 0.28

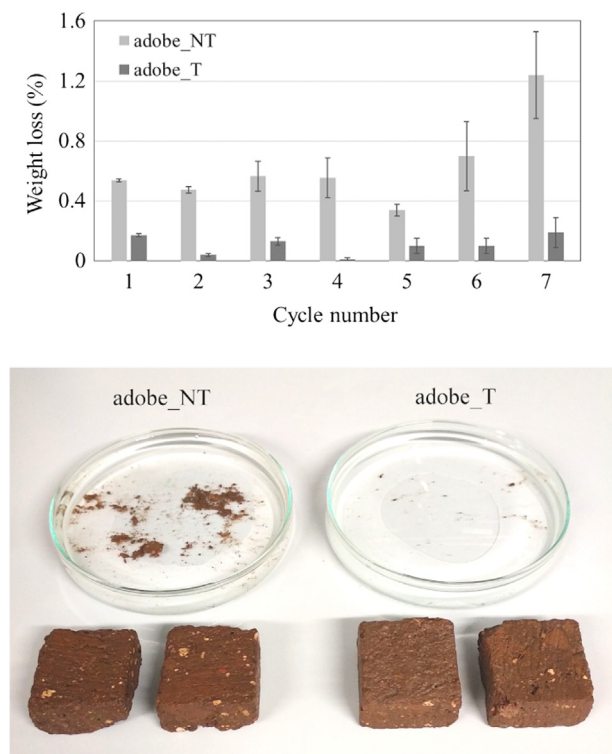


Fig. 9. (Top) Weight loss of adobe samples, untreated (NT), and treated with $\text{SiO}_2\text{-HPC-lime}$ (T), during wet/dry cycles. (Bottom) The adobe samples (untreated and treated) after the seventh wet/dry cycle. The untreated samples lost a significant amount of material, as opposed to those treated with the $\text{SiO}_2\text{-HPC-lime}$ formulation.

(see Table 3), indicating that the internal porosity of adobe was not altered, and the physico-chemical properties of the original material are preserved.

Lastly, drilling resistance measurements showed only a slight increase of the resistance for the treated samples (see Table 3).

It is important to notice that scotch tape tests, abrasion tests and wet/dry cycles revealed that some consolidation was obtained also applying only HPC (system HPC_T) or the two binary systems containing HPC (HPC-lime and $\text{SiO}_2\text{-HPC}$ system) (see Table 4), while the application of only SiO_2 or lime (system SiO_{2T} and lime_T) did not produce any significant consolidation effect. The system $\text{SiO}_2\text{-lime}$ is not applicable, as the two components flocculate in short times when combined without HPC.

Namely, treatment with HPC_T , HPC-lime and $\text{SiO}_2\text{-HPC}$ produced respectively total decohesion indexes of 1.9 ± 0.3 , 1.9 ± 0.3 and $1.8 \pm 0.3 \text{ mg/cm}^2$, and total abrasion coefficients of 152 ± 5 , 137 ± 6 and $145 \pm 5 \text{ cm}^2/\text{g}$. Besides, treatment with HPC_T produced a total weight loss after 7 wet/dry cycles of $2.02 \pm 0.05\%$. Therefore, it was concluded that the presence of hydroxypropyl cellulose led to an increase in surface cohesion, but further resistance was obtained by the application of the ternary system, confirming the importance of combining the three components, which burst the CSH formation *in situ*.

4. Conclusions

This work reports the first evidence, to the best of our knowledge, of the use of hybrid nano-composite materials for the consolidation of adobe. Namely, a ternary system ($\text{SiO}_2\text{-HPC-lime}$) was formulated, composed of materials that have full physico-chemical compatibility with those of adobe (as opposed to scarcely compatible adhesives [10–14], used in the adobe restoration practice). Each component was shown to play a role in the consolidation process, or in the stability of the ternary formulation. The use of nano-sized particles allowed the possibility to prepare stable and concentrated dispersions in water-solvent blends, avoiding the use of surfactants as stabilizers [33]. Our starting hypothesis was that the *in situ* reaction of the hybrid's components (SiO_2 and Ca(OH)_2 , in the presence of HPC) could lead to the formation of phases that consolidate the decohered adobe layers.

The physico-chemical characterization of the composite (by dynamic light scattering, electron microscopy, X-ray diffraction, and infrared spectroscopy) allowed to picture the interaction of the components. Namely, the interaction of highly reactive silica nanoparticles and calcium hydroxide nanoparticles led to the formation of calcium silicate hydrate (CSH), mimicking the chemistry of cement. The choice of an ethanol-water blend with ratio 4:1 allowed to obtain stable dispersions of the components in the desired amounts (ethanol prevents bridging and aggregation of the hydroxide platelets), and represented a balance between the need of avoiding aqueous media on water-sensitive substrates and the necessity of the presence of some water to trigger the alkaline activation of nanosilica and form CSH. To control and enhance the CSH reaction, nanoparticles were combined with a traditional consolidant and adhesive in conservation practice, *Klucel*[®]-G. In fact, cellulose derivatives are known to act as water regulators, binding water and then distributing it homogeneously over the solid phase, leading to an enhancement of CSH formation. Moreover, HPC is also essential in promoting the stability of SiO_2 and Ca(OH)_2 nanoparticles, preventing the sedimentation of the aggregates by increasing the viscosity of the dispersion, without affecting its applicability.

Our findings on the mutual interaction of the hybrid's components were complemented by the assessment of the formulation for adobe consolidation. The ternary formulation was applied on real adobe samples, exhibiting high porosity and surface powdering caused by natural aging (wind and water erosion). XRD measurements evidenced the formation of CSH within the pores of the treated adobe samples. Representative tests of exposure to environmental erosion (i.e. resistance to peeling, abrasion, and wet-dry cycles) showed improvement of the mechanical properties of adobe treated with the $\text{SiO}_2\text{-HPC-lime}$ formulation. In conclusion, consolidation was due to the formation of CSH, the main responsible for the setting process of cement, by reacting silica and lime nanoparticles in the presence of water and HPC. The ternary system was shown to grant better consolidation than the binary systems due to the presence of CSH promoted by the cellulose derivative. The composite particles penetrated homogeneously up to few millimeters from the surface, granting protection of the outer layers that are typically mostly degraded by erosion. Finally, the treatment did not induce discoloration of adobe, and left the

Table 4

Characterization of adobe samples, treated (T) with HPC_T , HPC-lime , and $\text{SiO}_2\text{-HPC}$. (NM = not measured).

	Total decohesion index after 3 peels (mg/cm^2)	Total abrasion coefficient after 3 cycles (cm^2/g)	Total weight loss after 7 wet/dry cycles (%)
Adobe_T(HPC_T)	1.9 ± 0.3	152 ± 5	2.02 ± 0.05
Adobe_T(HPC-lime)	1.9 ± 0.3	137 ± 6	NM
Adobe_T($\text{SiO}_2\text{-HPC}$)	1.8 ± 0.3	145 ± 5	NM

water permeability unaltered, both of which are essential requirements in stone consolidation, as opposed to conventional polymeric adhesives that are known to alter stone porosity and induce discoloration and flaking [12–14].

Overall, the ternary formulation was deemed as promising for the consolidation of earthen masonry, opening new perspectives in the use of nano-composites for immovable works of art. Future work should explore the use of this formulation as an additive in the adobe preparation, so as to obtain bricks that are able to stand weathering and erosion better than traditional recipes. This would represent a novel acceptable, inexpensive, and sustainable construction material alternative to cement in underdeveloped countries, where adobe is largely used.

Acknowledgments

All the authors gratefully acknowledge Dr. Yareli Jaidar (CNCPC-INAH and UNAM, Mexico City) for providing the adobe samples, Dr. Laura Chelazzi and Dr. Samuele Ciattini (CRIST, University of Florence) for assistance on XRD experiments, Dr. Costanza Montis for TEM experiments at Ce.M.E. (CNR, Florence), Dr. Silvia Rescic (CNR, Florence) for drilling measurements at ICVBC, Prof. Giovanni Gigli, Dr. Pietro Vannocci, Dr. Massimiliano Nocentini, Dr. Guia Cecchini and Dr. Teresa Salvatici (Department of Earth Sciences, University of Florence) for the preparation of the adobe samples and providing assistance on soil and samples characterization. Michael Persson (AkzoNobel-Nouryon) is gratefully acknowledged for providing the silica particles, and for the useful discussions. CGI and the European Union (NANORESTART project, Horizon 2020 research and innovation programme under grant agreement No 646063) are gratefully acknowledged for financial support.

References

- [1] E. Avrami, H. Guillaud, M. Hardy, *Terra literature review – an overview of research in earthen, Architect. Conserv.* (2008).
- [2] Terra 2008: The 10th International Conference on the Study and Conservation of Earthen Architectural Heritage, in: The Getty Conservation Institute, Los Angeles, CA, Bamako, Mali, 2008.
- [3] Terra 2000 Postprints: 8th International Conference on the Study and Conservation of Earthen Architecture, Torquay, Devon, UK, 2000.
- [4] E. Quagliarini, S. Lenci, The influence of natural stabilizers and natural fibres on the mechanical properties of ancient Roman adobe bricks, *J. Cult. Herit.* 11 (2010) 309–314, <https://doi.org/10.1016/j.culher.2009.11.012>.
- [5] C. Galán-Marín, C. Rivera-Gómez, J. Petric, Clay-based composite stabilized with natural polymer and fibre, *Constr. Build. Mater.* 24 (2010) 1462–1468, <https://doi.org/10.1016/j.conbuildmat.2010.01.008>.
- [6] G. Calatan, A. Hegyi, C. Dico, C. Mircea, Determining the optimum addition of vegetable materials in adobe bricks, *Procedia Technol.* 22 (2016) 259–265, <https://doi.org/10.1016/j.protcy.2016.01.077>.
- [7] D. Maskell, A. Heath, P. Walker, Inorganic stabilisation methods for extruded earth masonry units, *Constr. Build. Mater.* 71 (2014) 602–609, <https://doi.org/10.1016/j.conbuildmat.2014.08.094>.
- [8] L. Guerrero Baca, *Arquitectura en tierra. Hacia la recuperación de una cultura constructiva*, Apuntes 20 (2007) 182–201.
- [9] P. Baglioni, E. Carretti, D. Chelazzi, Nanomaterials in art conservation, *Nat. Nanotech.* 10 (2015) 287–290, <https://doi.org/10.1038/nnano.2015.38>.
- [10] K. Elert, E.S. Pardo, C. Rodríguez-Navarro, Alkaline activation as an alternative method for the consolidation of earthen architecture, *J. Cult. Herit.* 16 (2015) 461–469, <https://doi.org/10.1016/j.culher.2014.09.012>.
- [11] E. Doehe, C.A. Price, *Stone Conservation: An Overview of Current Research*, 2nd edition, 2011, [https://doi.org/10.1016/0006-3207\(70\)90031-5](https://doi.org/10.1016/0006-3207(70)90031-5).
- [12] M. Favaro, R. Mendichi, F. Ossola, S. Simon, P. Tomasin, P.A. Vigato, Evaluation of polymers for conservation treatments of outdoor exposed stone monuments. Part II: photo-oxidative and salt-induced weathering of acrylic-silicone mixtures, *Polym. Degrad. Stab.* 92 (2007) 335–351, <https://doi.org/10.1016/j.polydegstab.2006.12.008>.
- [13] O. Chiantore, M. Lazzari, Photo-oxidative stability of paraloid acrylic protective polymers, *Polymer (Guildf)*. 42 (2001) 17–27, [https://doi.org/10.1016/S0032-3861\(00\)00327-X](https://doi.org/10.1016/S0032-3861(00)00327-X).
- [14] D. Chelazzi, A. Chevalier, G. Pizzorusso, R. Giorgi, M. Menu, P. Baglioni, Characterization and degradation of poly(vinyl acetate)-based adhesives for canvas paintings, *Polym. Degrad. Stab.* 107 (2014) 314–320.
- [15] N. Bonelli, C. Montis, A. Mirabile, D. Berti, P. Baglioni, Restoration of paper artworks with microemulsions confined in hydrogels for safe and efficient removal of adhesive tapes, *Proc. Natl. Acad. Sci.* 115 (2018) 5932–5937, <https://doi.org/10.1073/pnas.1801962115>.
- [16] M. Baglioni, C. Montis, D. Chelazzi, R. Giorgi, D. Berti, P. Baglioni, Polymer film dewetting by water/surfactant/good-solvent mixtures: a mechanistic insight and its implications for the conservation of cultural heritage, *Angew. Chemie – Int. Ed.* 57 (2018) 7355–7359, <https://doi.org/10.1002/anie.201710930>.
- [17] D. Chelazzi, R. Giorgi, P. Baglioni, Microemulsions, micelles, and functional gels: how colloids and soft matter preserve works of art, *Angew. Chemie – Int. Ed.* 57 (2018) 7296–7303, <https://doi.org/10.1002/anie.201710711>.
- [18] M.J. Mosquera, D.M. de los Santos, T. Rivas, P. Sanmartín, B. Silva, New nanomaterials for protecting and consolidating stone, *J. Nano Res.* 8 (2009) 1–12, <https://doi.org/10.4028/www.scientific.net/JNanoR.8.1>.
- [19] M.A. Al-Dosari, S. Darwish, M.A. El-Hafez, N. Elmarzugi, N. Al-Mouallimi, S. Mansour, Effects of adding nanosilica on performance of ethylsilicat (TEOS) as consolidation and protection materials for highly porous artistic stone, *J. Mater. Sci. Eng. A* 6 (2016), <https://doi.org/10.17265/2161-6213/2016.7-8.002>.
- [20] I. De Rosario, F. Elhaddad, A. Pan, R. Benavides, T. Rivas, M.J. Mosquera, Effectiveness of a novel consolidant on granite: laboratory and in situ results, *Constr. Build. Mater.* 76 (2015) 140–149, <https://doi.org/10.1016/j.conbuildmat.2014.11.055>.
- [21] A. Zornoza-Indart, P. Lopez-Arce, Silica nanoparticles (SiO₂): influence of relative humidity in stone consolidation, *J. Cult. Herit.* 18 (2016) 258–270, <https://doi.org/10.1016/j.culher.2015.06.002>.
- [22] D. Chelazzi, G. Poggi, Y. Jaidar, N. Toccafondi, R. Giorgi, P. Baglioni, Hydroxide nanoparticles for cultural heritage: consolidation and protection of wall paintings and carbonate materials, *J. Colloid Interface Sci.* 392 (2013) 42–49, <https://doi.org/10.1016/j.jcis.2012.09.069>.
- [23] C. Rodríguez-Navarro, A. Suzuki, E. Ruiz-Agudo, Alcohol dispersions of calcium hydroxide nanoparticles for stone conservation, *Langmuir* 29 (2013) 11457–11470, <https://doi.org/10.1021/la4017728>.
- [24] M. Lanzón, J.A. Madrid, A. Martínez-Arredondo, S. Mónaco, Use of diluted Ca (OH)₂ suspensions and their transformation into nanostructured CaCO₃ coatings: a case study in strengthening heritage materials (stucco, adobe and stone), *Appl. Surf. Sci.* 424 (2017) 20–27, <https://doi.org/10.1016/j.apsusc.2017.02.248>.
- [25] C. Rodríguez-Navarro, E. Ruiz-Agudo, Nanolimes: from synthesis to application, *Pure Appl. Chem.* 90 (2018) 523–550, <https://doi.org/10.1515/pac-2017-0506>.
- [26] F. Ridi, E. Fratini, P. Baglioni, Cement: a two thousand year old nano-colloid, *J. Colloid Interface Sci.* 357 (2011) 255–264, <https://doi.org/10.1016/j.jcis.2011.02.026>.
- [27] S.A. Greenberg, Reaction between silica and calcium hydroxide solutions. Kinetics in the temperature range 30 to 85°, *J. Phys. Chem.* 65 (1961) 12–16, <https://doi.org/10.1021/j100819a005>.
- [28] D.R.G. Mitchell, I. Hinczak, R.A. Day, Interaction of silica fume with calcium hydroxide solutions and hydrated cement pastes, *Cem. Concr. Res.* 28 (1998) 1571–1584, [https://doi.org/10.1016/S0008-8846\(98\)00133-1](https://doi.org/10.1016/S0008-8846(98)00133-1).
- [29] L. Armelao, A. Bassan, R. Bertoncello, G. Biscontin, S. Daolio, A. Glisenti, Silica glass interaction with calcium hydroxide: a surface chemistry approach, *J. Cult. Herit.* 1 (2000) 375–384, [https://doi.org/10.1016/S1296-2074\(00\)01093-1](https://doi.org/10.1016/S1296-2074(00)01093-1).
- [30] K. Baltakys, R. Jaberthie, R. Siauciunas, R. Kaminskas, Influence of modification of SiO₂ on the formation of calcium silicate hydrate, *Mater. Sci.* 25 (2007) 663–670.
- [31] Q. Lin, X. Lan, Y. Li, Y. Ni, C. Lu, Y. Chen, Z. Xu, Preparation and characterization of novel alkali-activated nano silica cements for biomedical application, *J. Biomed. Mater. Res. – Part B Appl. Biomater.* 95 B (2010) 347–356, <https://doi.org/10.1002/jbm.b.31722>.
- [32] P. Baglioni, D. Chelazzi, R. Giorgi, G. Poggi, Colloid and materials science for the conservation of cultural heritage: cleaning consolidation, and deacidification, *Langmuir* 29 (2013) 5110–5122, <https://doi.org/10.1021/la304456n>.
- [33] V. Daniele, G. Taglieri, A. Gregori, Synthesis of Ca(OH)₂ nanoparticles aqueous suspensions and interaction with silica fume, *Adv. Mater. Res.* 629 (2013) 482–487, <https://doi.org/10.4028/www.scientific.net/AMR.629.482>.
- [34] M. Bouhicha, F. Aouissi, S. Kenai, Performance of composite soil reinforced with barley straw, *Cem. Concr. Compos.* 27 (2005) 617–621, <https://doi.org/10.1016/j.cemconcomp.2004.09.013>.
- [35] C.-M. Chan, Effect of natural fibres inclusion in clay bricks: physico-mechanical properties, *Int. J. Civ. Environ. Eng.* 5 (2011) 7–13.
- [36] F. Ridi, E. Fratini, R. Alfani, P. Baglioni, Influence of acrylic superplasticizer and cellulose-ether on the kinetics of tricalcium silicate hydration reaction, *J. Colloid Interface Sci.* 395 (2013) 68–74, <https://doi.org/10.1016/j.jcis.2012.12.048>.
- [37] P. Baglioni, D. Chelazzi, R. Giorgi, *Nanotechnologies in the Conservation of Cultural Heritage: A Compendium of Materials and Techniques*, Springer, Dordrecht Heidelberg London New York, 2015. doi: 10.1007/978-94-017-9303-2.
- [38] G. Poggi, N. Toccafondi, D. Chelazzi, P. Canton, R. Giorgi, P. Baglioni, Calcium hydroxide nanoparticles from solvothermal reaction for the deacidification of degraded waterlogged wood, *J. Colloid Interface Sci.* 473 (2016) 1–8, <https://doi.org/10.1016/j.jcis.2016.03.038>.
- [39] J. Nowakowska, *The Refractive Indices of Ethyl Alcohol and Water Mixtures*, Loyola University, Chicago, 1939.
- [40] T.A. Scott, Refractive index of ethanol-water mixtures and density and refractive index of ethanol-water-ethyl ether mixtures, *J. Phys. Chem.* 50 (1946) 406–412, <https://doi.org/10.1021/j150449a003>.
- [41] M. Drdacky, J. Lesak, S. Rescic, Z. Slížková, P. Tiano, J. Valach, Standardization of peeling tests for assessing the cohesion and consolidation characteristics of

- historic stone surfaces, *Mater. Struct.* (Dordrecht, Netherlands) 45 (2012) 505–520, <https://doi.org/10.1617/s11527-011-9778-x>.
- [42] AFNOR PR XP P13-901, Compressed Earth Blocks for Walls and Partitions: Definitions, Specifications, Test Methods, Conditions of Acceptance (2001).
 - [43] O. Izemmouren, A. Guettala, S. Guettala, Mechanical properties and durability of lime and natural pozzolana stabilized steam-cured compressed earth block bricks, *Geotech. Geol. Eng.* 33 (2015) 1321–1333, <https://doi.org/10.1007/s10706-015-9904-6>.
 - [44] ASTM D559/D559M, Standard Test Methods for Wetting and Drying Compacted Soil-Cement Mixtures, ASTM Int., West Conshohocken, Pa, 2015, pp. 1–6.
 - [45] BS EN 1925, Natural Stone Test Methods – Determination Of Water Absorption Coefficient By Capillarity (1999) pp. 1–10.
 - [46] N. Karagiannis, M. Karoglou, A. Bakolas, A. Moropoulou, Building materials capillary rise coefficient: concepts, determination and parameters involved, in: D.J. (Ed.), *New Approaches to Build. Pathol. Durability. Build. Pathol. Rehabil.*, Springer, Singapore, 2016, pp. 27–44, https://doi.org/10.1007/978-981-10-0648-7_2.
 - [47] M. Pamplona, M. Kocher, R. Snethlage, L.A. Barros, Drilling resistance: overview and outlook, *Zeitschrift Der Dtsch. Gesellschaft Für Geowissenschaften* 158 (2007) 665–679, <https://doi.org/10.1127/1860-1804/2007/0158-0665>.
 - [48] A. Samanta, D.K. Chanda, P.S. Das, J. Ghosh, A.K. Mukhopadhyay, A. Dey, Synthesis of nano calcium hydroxide in aqueous medium, *J. Am. Ceram. Soc.* 99 (2016) 787–795, <https://doi.org/10.1111/jace.14023>.
 - [49] S. Gunasekaran, G. Anbalagan, S. Pandi, Raman and infrared spectra of carbonates of calcite structure, *J. Raman Spectrosc.* 37 (2006) 892–899, <https://doi.org/10.1002/jrs.1518>.
 - [50] B. Plav, S. Kobe, B. Orel, Identification of crystallization forms of CaCO₃ with FTIR spectroscopy, *Kovine Zlitine Teh* 33 (1999) 517–521.
 - [51] N. Eguchi, K. Kawabata, H. Goto, Electrochemical polymerization of 4,4-dimethyl-2,2'-bithiophene in concentrated polymer liquid crystal solution, *J. Mater. Sci. Chem. Eng.* 05 (2017) 64–70, <https://doi.org/10.4236/msce.2017.52007>.
 - [52] D.M. Sudarsan Reddy, K. Prabhakar, M.N. Madhusudana Rao, K. Suhasini, V. Naga Maheswara Reddy, P. Kumara Babu, K. Sudhakar, A. Chandra Babu, M.C.S. Subha, K. Chowdaji Rao, Development and characterization of hydroxy propyl cellulose/poly(vinyl alcohol) blends and their physico-chemical studies, *Indian J. Adv. Chem. Sci.* 2 (1) (2013) 38–45.
 - [53] W.A.P.J. Premaratne, W.M.G.I. Priyadarshana, S.H.P. Gunawardena, A.A.P. De Alwis, Synthesis of nanosilica from paddy husk ash and their surface functionalization, *J. Sci. Univ. Kelaniya Sri Lanka* 8 (2013) 33–48, <https://doi.org/10.4038/josuk.v8i0.7238>.
 - [54] D.M. Marzouqa, M.B. Zughul, M.O. Taha, H.A. Hodali, Effect of particle morphology and pore size on the release kinetics of ephedrine from mesoporous MCM-41 materials, *J. Porous Mater.* 19 (2012) 825–833, <https://doi.org/10.1007/s10934-011-9537-y>.
 - [55] S. Grangeon, F. Claret, C. Roos, T. Sato, S. Gaboreau, Y. Linard, Structure of nanocrystalline calcium silicate hydrates: Insights from X-ray diffraction, synchrotron X-ray absorption and nuclear magnetic resonance, *J. Appl. Crystallogr.* 49 (2016) 771–783, <https://doi.org/10.1107/S1600576716003885>.
 - [56] Q. Lin, Z. Xu, X. Lan, Y. Ni, C. Lu, The reactivity of nano silica with calcium hydroxide, *J. Biomed. Mater. Res. – Part B Appl. Biomater.* 99 B (2011) 239–246, <https://doi.org/10.1002/jbm.b.31891>.
 - [57] S. Grangeon, F. Claret, C. Lerouge, F. Warmont, T. Sato, S. Anraku, C. Numako, Y. Linard, B. Lanson, On the nature of structural disorder in calcium silicate hydrates with a calcium/silicon ratio similar to tobermorite, *Cem. Concr. Res.* 52 (2013) 31–37, <https://doi.org/10.1016/j.cemconres.2013.05.007>.
 - [58] S. Grangeon, F. Claret, Y. Linard, C. Chiaberge, X-ray diffraction: a powerful tool to probe and understand the structure of nanocrystalline calcium silicate hydrates, *Acta Crystallogr. Sect. B Struct. Sci. Cryst. Eng. Mater.* 69 (2013) 465–473, <https://doi.org/10.1107/S2052519213021155>.
 - [59] S. Wang, X. Peng, L. Tang, L. Zeng, C. Lan, Influence of inorganic admixtures on the 11 Å-tobermorite formation prepared from steel slags: XRD and FTIR analysis, *Constr. Build. Mater.* 60 (2014) 42–47, <https://doi.org/10.1016/j.conbuildmat.2014.03.002>.
 - [60] X. Guo, F. Meng, H. Shi, Microstructure and characterization of hydrothermal synthesis of Al-substituted tobermorite, *Constr. Build. Mater.* 133 (2017) 253–260, <https://doi.org/10.1016/j.conbuildmat.2016.12.059>.
 - [61] E. Tajuelo Rodriguez, I.G. Richardson, L. Black, E. Boehm-Courjault, A. Nonat, J. Skibsted, Composition, silicate anion structure and morphology of calcium silicate hydrates (C-S-H) synthesised by silica-lime reaction and by controlled hydration of tricalcium silicate (C₃S), *Adv. Appl. Ceram.* 114 (2015) 362–371, <https://doi.org/10.1179/1743676115Y.0000000038>.
 - [62] C. Graf, Q. Gao, I. Schütz, C.N. Noufele, W. Ruan, U. Posselt, E. Korotianskiy, D. Nordmeyer, F. Rancan, S. Hadam, A. Vogt, J. Lademann, V. Hauke, E. Rühl, Surface functionalization of silica nanoparticles supports colloidal stability in physiological media and facilitates internalization in cells, *Langmuir* 28 (2012) 7598–7613, <https://doi.org/10.1021/la204913t>.
 - [63] G. Poggi, N. Toccacfondi, L.N. Melita, J.C. Knowles, L. Bozec, R. Giorgi, P. Baglioni, Calcium hydroxide nanoparticles for the conservation of cultural heritage: new formulations for the deacidification of cellulose-based artifacts, *Appl. Phys. A Mater. Sci. Process.* 114 (2014) 685–693, <https://doi.org/10.1007/s00339-013-8172-7>.
 - [64] G. Åkerlöf, Dielectric constants of some organic solvent-water mixtures at various temperatures, *J. Am. Chem. Soc.* 54 (1932) 4125–4139, <https://doi.org/10.1021/ja01350a001>.
 - [65] T. Moriyoshi, T. Ishii, Y. Tamai, M. Tado, Static dielectric constants of water + ethanol and water + 2-methyl-2-propanol mixtures from 0.1 to 300 MPa at 298.15 K, *J. Chem. Eng. Data.* 35 (1990) 17–20, <https://doi.org/10.1021/je00059a005>.
 - [66] J. Gregory, Flocculation by polymers and polyelectrolytes, in: T.F. Tadros (Ed.), *Solid/Liquid Dispersions*, Academic Press, London, UK, 1987, pp. 163–180.
 - [67] A.V. Delgado, Interfacial electrokinetics and electrophoresis, in: *Surfactant Sci. Ser.*, CRC Press, 2001, pp. 1–1016.
 - [68] F. Bouville, S. Deville, Dispersion of boron nitride powders in aqueous suspensions with cellulose, *J. Am. Ceram. Soc.* 97 (2014) 394–398, <https://doi.org/10.1111/jace.12653>.
 - [69] D.L. Berthier, A. Herrmann, L. Ouali, Synthesis of hydroxypropyl cellulose derivatives modified with amphiphilic diblock copolymer side-chains for the slow release of volatile molecules, *Polym. Chem.* 2 (2011) 2093–2101, <https://doi.org/10.1039/c1py00195g>.
 - [70] P.W. Brown, C.R. Robbins, J.R. Clifton, Adobe II: factors affecting the durability of adobe structures, *Stud. Conserv.* 24 (1979) 23–39, <https://doi.org/10.1179/sic.1979.003>.
 - [71] M. Hamiane, I. Djefour, H. Merabet, D. Bouallala, A. Zekagh, Y. Turki, M. Saidi, Design of adobe bricks of local raw materials for use in the monuments of earthen architecture (case of Adrar Hospital) Algeria, *Civ. Eng. Archit.* 4 (2016) 147–152, <https://doi.org/10.13189/cea.2016.040401>.
 - [72] R.S. Berns, D.M. Reiman, Color managing the third edition of Billmeyer and Saltzman's Principles of Color Technology, *Color Res. Appl.* 27 (2002) 360–373, <https://doi.org/10.1002/col.10083>.
 - [73] P. Croveri, L. Dei, R. Giorgi, B. Salvadori, Consolidation of globigerina limestone (Malta) by means of inorganic treatments: preliminary results, in: D. Kwiatkowski, R. Lofvendahl (Eds.), *Proc. 10th Int. Congr. Deterior. Conserv. Stone 1*, Stock, 2004, p. 463.
 - [74] L. Dei, B. Salvadori, Nanotechnology in cultural heritage conservation: nanometric slaked lime saves architectonic and artistic surfaces from decay, *J. Cult. Herit.* 7 (2006) 110–115, <https://doi.org/10.1016/j.culher.2006.02.001>.
 - [75] G. Ziegenbalg, Colloidal calcium hydroxide – a new material for consolidation and conservation of carbonatic stones, *Proc. 11th Int. Congr. Deterior. Conserv. Stone*, 15–20 Sept. 2008, Torun, Pol., 2008.
 - [76] P. D'Armada, E. Hirst, Nano-lime for consolidation of plaster and stone, *J. Archit. Conserv.* 1 (2012) 63–80, <https://doi.org/10.1080/13556207.2012.10785104>.
 - [77] A. Daehne, C. Herm, Calcium hydroxide nanosols for the consolidation of porous building materials – results from EU-STONECORE, *Herit. Sci.* 1 (2013) 11–20, <https://doi.org/10.1186/2050-7445-1-11>.
 - [78] I. Ntali, M.L. Saladino, F. Andriolo, D. Chillura Martino, E. Caponetti, E. Carretti, L. Dei, Consolidation and protection by nanolime: recent advances for the conservation of the graffiti, Carceri dello Steri Palermo and of the 18th century lunettes, SS. Giuda e Simone Cloister, Corniola (Empoli), *J. Cult. Herit.* 1 (2014) 151–158, <https://doi.org/10.1016/j.culher.2013.03.002>.
 - [79] S. Del Buffa, E. Fratini, F. Ridi, A. Faraone, P. Baglioni, State of water in hydrating tricalcium silicate pastes: the effect of a cellulose ether, *J. Phys. Chem. C* 120 (2016) 7612–7620, <https://doi.org/10.1021/acs.jpcc.6b00691>.